Preparation, Electronic Structure, and Photoluminescence Properties of Eu^{2+}- and Ce^{3+}/Li^{+}-Activated Alkaline Earth Silicon Nitride $MSiN_2$ (M = Sr, Ba)

C. J. Duan,[†] X. J. Wang,[‡] W. M. Otten,[†] A. C. A. Delsing,[†] J. T. Zhao,[‡] and H. T. Hintzen*,[†]

Material and Devices for Sustainable Energy Technologies, Department of Chemical Engineering and Chemistry, Eindhoven University of Technology, P.O. Box 513, 5600 MB Eindhoven, The Netherlands, State Key Laboratory of High Performance Ceramics and Superfine Microstructure, Shanghai Institute of Ceramics, Chinese Academy of Sciences, Shanghai 200050, People's Republic of China

Received July 17, 2007. Revised Manuscript Received November 23, 2007

The electronic structure of alkaline-earth silicon nitride $MSiN_2$ (M = Sr, Ba) was calculated using the CASTEP code. $BaSiN_2$ is calculated to be an intermediate band gap semiconductor with a direct energy gap of about 2.9 eV, while $SrSiN_2$ is an intermediate band gap semiconductor with an indirect energy gap of about 3.0 eV. As expected, the calculated optical band gaps of $MSiN_2$ (M = Ba, Sr) are lower compared to the experimentally determined values (about 4.1 eV for $BaSiN_2$ and 4.2 eV for $SrSiN_2$). In addition, the luminescence properties of Eu^{2+} and Ce^{3+} in $MSiN_2$ (M = Sr, Ba) have been studied. $Ba_{1-x}Eu_xSiN_2$ ($0 < x \leq 0.1$) shows a broad emission band in the wavelength range of 500–750 nm with maxima from about 600 to 630 nm with increaseing Eu^{2+} concentration, while $Sr_{1-x}Eu_xSiN_2$ ($0 < x \leq 0.1$) shows a broad emission band in the wavelength range of 550–850 nm with maxima from 670 to 685 nm with increasing Eu^{2+} concentration. The high absorption and strong excitation bands of $M_{1-x}Eu_xSiN_2$ ($0 < x \leq 0.1$; M = Sr, Ba) in the wavelength range of 300–530 m are very favorable properties for application as light-emitting-diode conversion phosphors. Ce^{3+}- and Li^{+}- codoped $MSiN_2$ (M = Sr, Ba) exhibits a broad emission band in the wavelength range of 400–700 nm with a peak center at about 485 nm for $BaSiN_2$ and about 535 nm for $SrSiN_2$. A comparison is made between the luminescence properties of Eu^{2+} and Ce^{3+} in the Sr versus Ba compounds. The long-wavelength excitation and emission of Eu^{2+} and Ce^{3+} ions in the host of $MSiN_2$ (M = Sr, Ba) are attributed to the effect of a high covalency and a large crystal field splitting on the 5d bands of Eu^{2+} and Ce^{3+} in the nitrogen coordination environment.

1. Introduction

Nitridosilicates, oxonitridosilicates, or oxonitridoaluminosilicates, which are related to oxosilicates by formal exchanges of oxygen by nitrogen or/and silicon by aluminum, are of great interest owing to their outstanding thermal, chemical, and mechanical stability and structural diversity.[1,2] Recently, these compounds have been extensively studied as host lattices for phosphors, which exhibit unusual, interesting luminescence properties when activated by rare earth ions, such as $M_2Si_5N_8$:Eu^{2+}/Ce^{3+},[3–8] $MSi_2O_{2-\delta}N_{2+2/3\delta}$:$Eu^{2+}/Ce^{3+}$ (M = Ca, Sr, Ba),[9–11] $CaSiN_2$:Eu^{2+}/Ce^{3+},[12,13] $MgSiN_2$:Eu^{2+},[14,15] $MYSi_4N_7$:Eu^{2+}/Ce^{3+} (M = Sr, Ba),[16,17] $MSi_xAl_{2-x}O_{4-x}N_x$:Eu^{2+} (M = Ca, Sr, Ba),[18] α-SiAlON:RE (RE = Eu^{2+}, Ce^{3+}, Yb^{2+}, Tb^{3+}, Pr^{3+}, Sm^{3+}),[19–24]

* To whom correspondence should be addressed. Tel.: +31-40-2473113. Fax: +31-40-2445619. E-mail: h.t.hintzen@tue.nl.
† Eindhoven University of Technology.
‡ Chinese Academy of Sciences.

(1) Schnick, W. *Int. J. Inorg. Mater.* **2001**, *3*, 1267.
(2) Schnick, W.; Huppertz, H. *Chem.—Eur. J.* **1997**, *3*, 679.
(3) Hoppe, H. A.; Lutz, H.; Morys, P.; Schnick, W.; Seilmeier, A. *J. Phys. Chem. Solids* **2000**, *61*, 2001.
(4) van Krevel, J. W. H. Ph.D. Thesis, Eindhoven University of Technology, 2000.
(5) Li, Y. Q.; de With, G.; Hintzen, H. T. *J. Lumin.* **2006**, *116*, 107.
(6) Li, Y. Q.; van Steen, J. E. J.; van Krevel, J. W. H.; Botty, G.; Delsing, A. C. A.; DiSalvo, F. J.; de With, G.; Hintzen, H. T. *J. Alloys Compd.* **2006**, *417*, 273.
(7) Xie, R. J.; Hirosaki, N.; Suehiro, T.; Xu, F. F.; Mitomo, M. *Chem. Mater.* **2006**, *18*, 5578.
(8) Piao, X. Q.; Horikawa, T.; Hanzawa, H.; Machida, K. *Appl. Phys. Lett.* **2006**, *88*, 161908.
(9) Li, Y. Q.; de With, G.; Hintzen, H. T. *J. Mater. Chem.* **2005**, *15*, 4492.
(10) Li, Y. Q.; Delsing, A. C. A.; de With, G.; Hintzen, H. T. *Chem. Mater.* **2005**, *15*, 4492.
(11) Bachmann, V.; Jüstel, T.; Meijerink, A.; Ronda, C. J.; Schmidt, P. *J. Lumin.* **2006**, *121*, 441.
(12) Lee, S. S.; Lim, S.; Sun, S. S.; Wager, J. F. *Proc. SPIE−Int. Soc. Opt. Eng.* **1997**, *3241*, 75.
(13) Le, T. R.; Cheetham, A. K. *Chem. Phys. Lett.* **2006**, *423*, 354.
(14) Dubrovskii, G. P.; Zykov, A. M.; Chernovets, B. V. *Izv. Akad. Nauk SSSR, Neorg. Mater.* **1981**, *17* (8), 1421.
(15) Gaido, G. K.; Dubrovskii, G. P.; Zykov, A. M. *Izv. Akad. Nauk SSSR, Neorg. Mater.* **1974**, *10* (3), 564.
(16) Li, Y. Q.; Fang, C. M.; de With, G.; Hintzen, H. T. *J. Solid State Chem.* **2004**, *177*, 4687.
(17) Li, Y. Q.; de With, G.; Hintzen, H. T. *J. Alloys. Compd.* **2004**, *385*, 1.
(18) Li, Y. Q.; de With, G.; Hintzen, H. T. *J. Electrochem. Soc.* **2006**, *153*, G278.
(19) Xie, R. J.; Mitomo, M.; Uheda, K.; Xu, F. F.; Akimune, Y. *J. Am. Ceram. Soc.* **2002**, *85*, 1229.
(20) Xie, R. J.; Hirosaki, N.; Mitomo, M.; Yamamoto, Y.; Suehiro, T.; Sakuma, K. *J. Phys. Chem. B* **2004**, *108*, 12027.
(21) Xie, R. J.; Hirosaki, N.; Sakuma, K.; Yamamoto, Y.; Mitomo, M. *Appl. Phys. Lett.* **2004**, *84*, 5404.
(22) Xie, R. J.; Hirosaki, N.; Mitomo, M.; Uheda, K.; Suehiro, T.; Xu, X.; Yamamoto, Y.; Sekiguchi, T. *J. Phys. Chem. B* **2005**, *109*, 9490.

10.1021/cm701875e CCC: $40.75
Published on Web 01/03/2008

β-SiAlON:Eu^{2+},[25] and $CaAlSiN_3$:Eu^{2+}.[26] Most importantly, these phosphors emit visible light efficiently under near-ultraviolet or blue-light irradiation and have superior thermal and chemical stability to their oxide and sulfide counterparts, allowing them to be used as down-conversion luminescent materials for white light-emitting diodes (LEDs). A series of compounds with the composition $MSiN_2$ (M = Be,[27] Mg,[28,29] Ca,[30] Sr,[31] Ba[32]) have been reported for many years, but for these only the ordered wurtzite structures of $BeSiN_2$[27] and $MgSiN_2$[28] with three-dimensional frameworks of vertex-sharing SiN_4 tetrahedra were determined. However, recently, the structure of $MSiN_2$ with large M ions (M = Ca, Sr, Ba) has been solved for single crystals, which were grown from molten sodium at 900–1100 °C.[33] $BaSiN_2$ crystallizes in space group *Cmca*. The structure consists of pairs of SiN_4 tetrahedra edge-linked to form bow-tie-shaped Si_2N_6 dimers, which share vertexes to form layers, and has no analogue in oxide chemistry. $SrSiN_2$ has a distorted form of this structure and crystallizes in space group $P21/c$. In $MSiN_2$ (M = Sr, Ba), there is only one crystallographic M site with 8-fold nitrogen coordination. To our knowledge, no investigations have been focused on studying the photoluminescence properties of rare earth in the hosts of $MSiN_2$ (M = Sr, Ba) yet. Here, we report the electronic structure of the undoped and the photoluminescence properties of Eu^{2+}- and Ce^{3+}/Li^+- activated alkaline earth silicon nitride $MSiN_2$ (M = Sr, Ba) materials.

2. Experimental Section

2.1. Starting Materials. The binary nitride precursors SrN_x ($x \approx 0.6$–0.66), BaN_x ($x \approx 0.6$–0.66), and EuN ($x \approx 0.94$) were preprepared by the reaction of pure strontium metal (Aldrich, 99.9%, pieces), barium metal (Aldrich, 99.9%, pieces), and Eu metal (Csre, 99.9%, lumps) under flowing dried nitrogen at 800, 550, and 800 °C, respectively, for 8–16 h in a horizontal tube furnace. In addition, α-Si_3N_4 powder (Permascand, P95H; α content, 93.2%; oxygen content, ~1.5%), Ce (Alfa, >99%, lumps), and Li (Merck, >99%, lumps) are used as the as-received raw materials.

2.2. Synthesis of Undoped, Eu^{2+}- and Ce^{3+}/Li^+-Doped $MSiN_2$ (M = Sr, Ba). Polycrystalline $M_{1-x}Eu_xSiN_2$ ($0 \le x \le 0.1$) and $M_{1-2x}Ce_xLi_xSiN_2$ ($0 \le x \le 0.05$) powders were prepared by a solid-state reaction method at high temperatures. The appropriate amounts of metal (Ce, Li), SrN_x, BaN_x, and EuN_x as well as α-Si_3N_4 powders were weighed out and subsequently mixed and ground together with an agate mortar. The powder mixtures were then transferred into molybdenum crucibles. All processes were carried out in a purified-nitrogen-filled glovebox. Subsequently, those powder mixtures were fired in a horizontal tube furnace at 1250 °C for 16 h under a flowing 90% N_2–10% H_2 atmosphere. After firing, the samples were gradually cooled down to room temperature in the furnace. There was no apparent reaction of the prepared nitrides with the Mo crucibles.

2.3. X-Ray Diffraction (XRD) Data Collection. All measurements were performed on finely ground samples, which were analyzed by X-ray powder diffraction (Rigaku, D/MAX-B) using Cu Kα radiation at 40 kV and 30 mA with a graphite monochromator. The phase formation is checked by the normal scan (0.6°/min) in the range of 10–90° 2θ. All the XRD measurements were performed at room temperature in the air. All the samples are shown to be pure phases, and the powder X-ray diffraction patterns of undoped or doped $SrSiN_2$ and $BaSiN_2$ samples are in good agreement with the reported powder patterns in JCPDS 22-1438 and 36-1257, respectively. The powder X-ray diffraction patterns of undoped or doped $SrSiN_2$ and $BaSiN_2$ samples are also the same as the patterns obtained for single crystal studies (ref 33).

2.4. Optical Measurements. The diffuse reflectance, emission, and excitation spectra of the samples were measured at room temperature with a Perkin-Elmer LS 50B spectrophotometer equipped with a Xe flash lamp. The reflection spectra were calibrated with the reflection of black felt (reflection 3%) and white barium sulfate ($BaSO_4$, reflection ~100%) in the wavelength region of 230–700 nm. The excitation and emission slits were set at 15 nm. The emission spectra were corrected by dividing the measured emission intensity by the ratio of the observed spectrum of a calibrated W lamp and its known spectrum from 300 to 900 nm. Excitation spectra were automatically corrected for the variation in the lamp intensity by a second photomultiplier and a beam splitter. All the luminescence spectra were measured with a scan speed of 400 nm/min at room temperature in the air. The quantum efficiency (Q.E.) of the $MSiN_2$:Eu^{2+} (M = Sr, Ba) phosphors was determined under an excitation of 450 nm as compared to the commercial LED phosphor Ce^{3+}-doped yttrium aluminum garnet (YAG:Ce^{3+}). In order to do it, the light output (L.O.; i.e., integrated intensity) of the $MSiN_2$:Eu^{2+} and YAG:Ce^{3+} phosphors under an excitation of 450 nm and the absorption percentage (Abs.) of them at 450 nm should be determined in first step. Then, the quantum efficiency of the $MSiN_2$:Eu^{2+} (M = Sr, Ba) phosphors was determined by using the following function:

$$\text{Q.E.}(MSiN_2{:}Eu^{2+}) = \text{Q.E.}(YAG{:}Ce^{3+}) \times \frac{\text{L.O.}(MSiN_2{:}Eu^{2+})}{\text{L.O.}(YAG{:}Ce^{3+})} \times \frac{\text{Abs}(YAG{:}Ce^{3+})}{\text{Abs}(MSiN_2{:}Eu^{2+})} \quad (1)$$

2.5. Electronic Structure Calculations. The calculations of the electronic structures for $SrSiN_2$ and $BaSiN_2$ were carried out with density functional theory and performed with the CASTEP code.[34,35] The generalized gradient approximations (GGA) were chosen for the theoretical basis of density function. The code used the band-by-band conjugate-gradient technique to minimize the total energy with respect to the plane-wave coefficient. Two steps were necessary for calculating the electronic band structure of $MSiN_2$ (M = Sr, Ba). The first step was to optimize their crystal structure using the crystallographic data reported in the literature.[33] There is only a small difference between the experimental lattice parameters and

(23) Xie, R. J.; Hirosaki, N.; Mitomo, M.; Takahashi, K.; Sakuma, K. *Appl. Phys. Lett.* **2006**, *88*, 101104.
(24) van Krevel, J. W. H.; van Rutten, J. W. T.; Mandal, H.; Hintzen, H. T.; Metselaar, R. *J. Solid State Chem.* **2002**, *165*, 19.
(25) Hirosaki, N.; Xie, R. J.; Kimoto, K.; Sekiguchi, T.; Yamamoto, Y.; Suehiro, T.; Mitomo, M. *Appl. Phys. Lett.* **2005**, *86*, 211905.
(26) Uheda, K.; Hirosaki, N.; Yamamoto, Y.; Naoto, A.; Nakajima, T.; Yamamoto, H. *Electrochem. Solid State Lett.* **2006**, *9*, H22.
(27) Rabenau, A.; Eckerlin, P. *Naturwissenschaften* **1959**, *46*, 106.
(28) David, J.; Laurent, Y.; Lang, J. *Bull. Soc. Fr. Mineral. Cristallogr.* **1970**, *93*, 153.
(29) Bruls, R. J.; Hintzen, H. T.; Metselaar, R.; Loong, C. K. *J. Phys. Chem. Solids* **2000**, *61*, 1285.
(30) Laurent, Y.; Lang, J. *C. R. Acad. Sci. Paris* **1966**, *262*, 103.
(31) Gaudé, J.; Lang, J. *C. R. Acad. Sci. Paris* **1969**, *268*, 1785.
(32) Morgan, P. E. D. *J. Mater. Sci. Lett.* **1984**, *3*, 131.
(33) Gál, Z. A.; Mallinson, P. M.; Orchard, H. J.; Clarke, S. J. *Inorg. Chem.* **2004**, *43*, 3998.
(34) Segall, M.; Linda, P.; Probert, M.; Pickard, C.; Hasnip, P.; Clark, S.; Payne, M. *Materials Studio CASTEP*, version 2.2; Accelrys: San Diego, CA, 2002.
(35) Segall, M.; Linda, P.; Probert, M.; Pickard, C.; Hasnip, P.; Clark, S.; Payne, M. *J. Phys.: Condens. Mater.* **2002**, *14*, 2717.

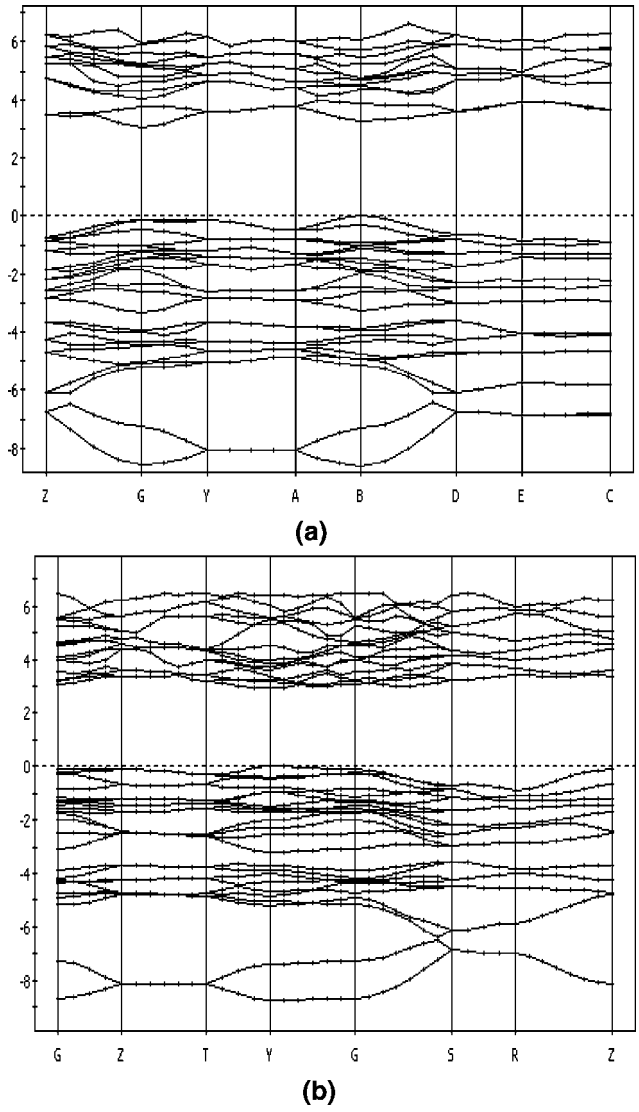

Figure 1. Band structures of $MSiN_2$: (a) M = Sr, (b) M = Ba.

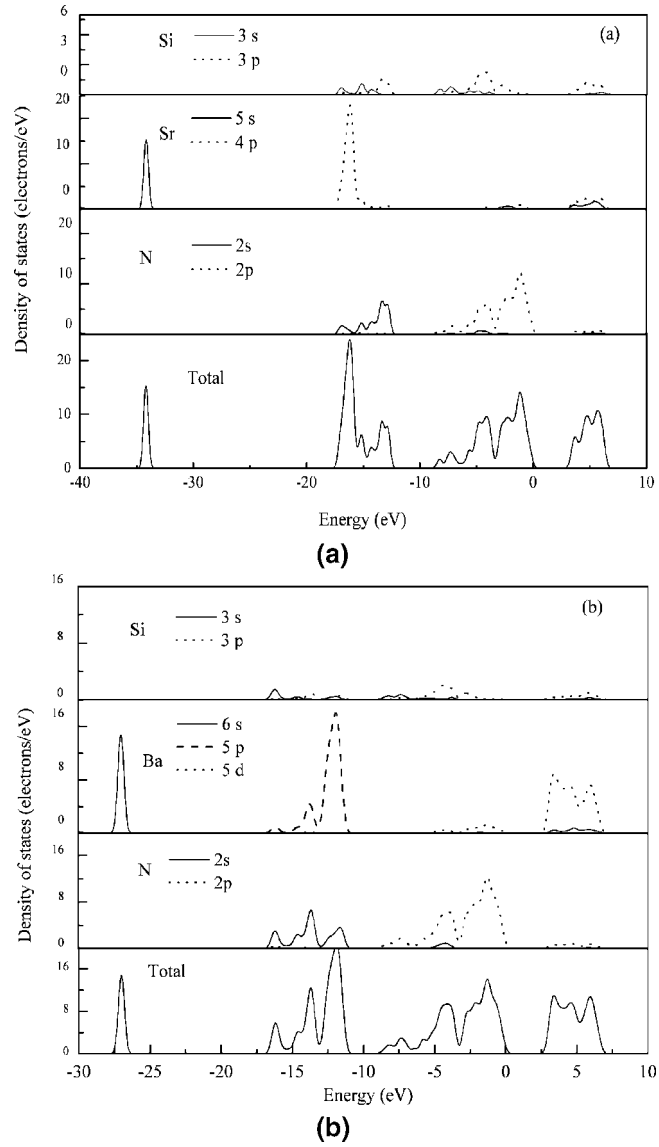

Figure 2. Total and partial density of states of $MSiN_2$: (a) M = Sr, (b) M = Ba.

calculated ones after the optimization of crystal structure, which will not be indicated here. The second step was to calculate the band structure and density of states of $MSiN_2$ (M = Sr, Ba) for the optimized structure. Lattice parameter and atomic coordinates were fixed at the values obtained by the crystal structure optimization process in the first step. For the two steps, the basic parameters were chosen as follows in setting up the CASTEP run: the kinetic energy cutoff = 250 eV, k-point spacing = 0.04 $Å^{-1}$, sets of k points = 5 × 3 × 5 for $SrSiN_2$ and 4 × 2 × 2 for $BaSiN_2$, SCF tolerance thresholds= 1.0×10^{-6} eV/atom, and space representation = reciprocal.

3. Results and Discussion

3.1. The Electronic Structure of $MSiN_2$ (M = Sr, Ba). Figure 1, parts a and b show the band structures of $SrSiN_2$ and $BaSiN_2$, respectively. As shown in Figure 1, $SrSiN_2$ shows an indirect optical band gap and $BaSiN_2$ shows a direct optical band gap. The gap between the lowest energy of the conduction band and the highest energy of the valence band is about 2.9 eV for $BaSiN_2$ and 3.0 eV for $SrSiN_2$, which is lower compared to the experimentally determined values (about 4.1 eV for $BaSiN_2$ and 4.2 eV for $SrSiN_2$; see section 3.2). This difference is normal as the GGA underestimates the size of the band gap.[36] $MSiN_2$ (M = Sr, Ba) thus belongs to the category of materials with large band gaps that are usually good hosts for many luminescent ions. The large band gap helps to accommodate both the ground and excited states within the band gap. Figure 2, parts a and b show the total and partial density of states of $SrSiN_2$ and $BaSiN_2$, respectively. For both $BaSiN_2$ and $SrSiN_2$, the top of the valence band is dominated by N 2p states. The bottom of the conduction band is dominated by the Ba 5d states for $BaSiN_2$, while the bottom of the conduction band of $SrSiN_2$ is mainly composed of Sr 5s, 4p, and Si 3p states.

3.2. Diffuse Reflection Spectra of Undoped, Eu^{2+}- and Ce^{3+}/Li^{+}-Doped $MSiN_2$ (M = Sr, Ba). Figure 3 shows the diffuse reflection spectra of undoped and Eu^{2+}-doped $MSiN_2$ (M = Sr, Ba). Both undoped and Eu^{2+}-doped samples show a remarkable drop in reflection in the UV range around 300 nm, corresponding to the valence-to-conduction band transitions of the $MSiN_2$ host lattice. The intense reflection in the visible spectral range is in agreement with the observed

(36) Jones, R. O.; Gunnarsson, O. *Rev. Mod. Phys.* **1989**, *61*, 689.

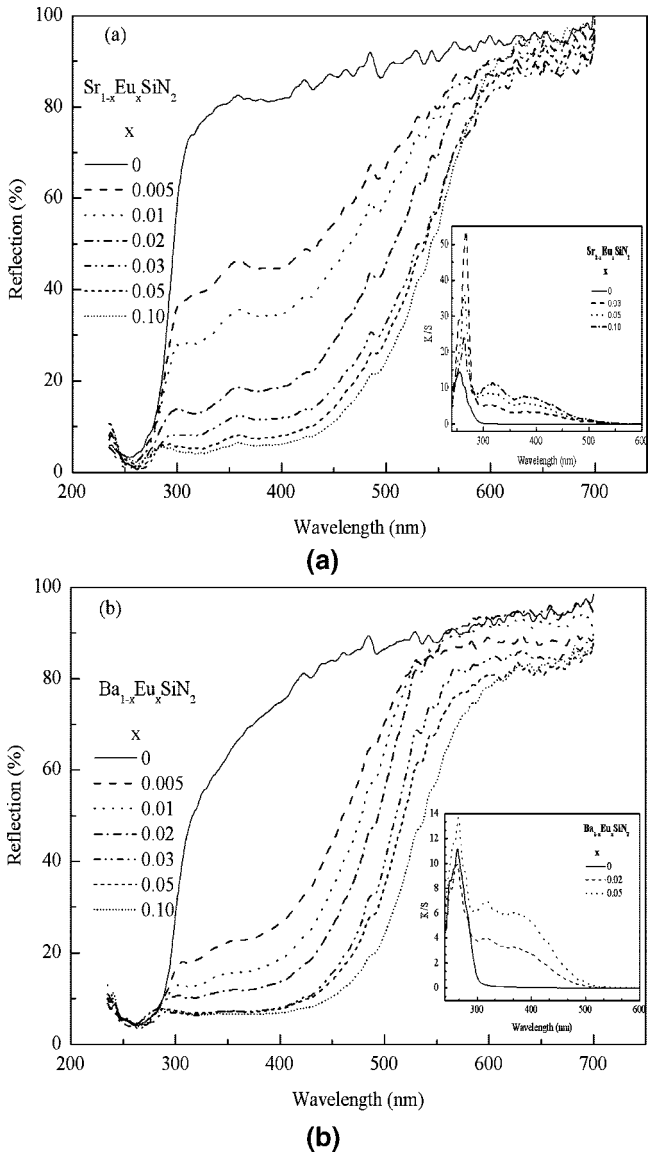

Figure 3. Diffuse reflection spectra of $M_{1-x}Eu_xSiN_2$: (a) M = Sr, (b) M = Ba. (The insets show the absorption spectra of $M_{1-x}Eu_xSiN_2$ as calculated by the Kubelka–Munk formula.)

gray-white daylight color for undoped $MSiN_2$. In order to better localize the thresholds for host lattice absorption and the absorption by Eu^{2+}, the absorption spectra of $M_{1-x}Eu_xSiN_2$ ($0 \le x \le 0.1$) were obtained from the reflection spectra by using the Kubelka–Munk function:[37]

$$F(R) = (1-R)^2/2R = K/S \qquad (2)$$

R, K, and S are the reflection, the absorption, and the scattering coefficient, respectively. The absorption spectra of $M_{1-x}Eu_xSiN_2$ ($0 \le x \le 0.1$) derived with the Kubelka–Munk function are shown in the insets of Figure 2. The value of the optical band gap is calculated to be about 4.2 eV (i.e., 295 nm) for $SrSiN_2$ and 4.1 eV (i.e., 303 nm) for $BaSiN_2$ by extrapolating the Kubelka–Munk function to $K/S = 0$. In addition, two broad absorption bands can also be seen from the absorption spectra of the high-Eu^{2+}-concentration samples. One is in the wavelength range of 350–530 nm; another is a short-wavelength absorption band in the wavelength range of 300–350 nm. The two broad absorption bands both can be attributed to the absorption by Eu^{2+} ions due to the absence of them in undoped $MSiN_2$ samples. As expected, the intensities of them increase for higher Eu^{2+} concentrations. In contrast to the undoped samples, the daylight color of $M_{1-x}Eu_xSiN_2$ shows light orange to orange for M = Sr and yellow to orange for M = Ba, varying with the Eu^{2+} concentration ($0 < x \le 0.1$) as a result of a strong absorption in the visible range 420–530 nm.

Figure 4 shows the typical diffuse reflection spectra of Ce^{3+} and Li^+-codoped $MSiN_2$ (M = Sr, Ba) samples. The diffuse reflection spectra of undoped samples were also plotted as a comparison. The intense reflection in the visible spectral range is in agreement with the observed gray-white daylight color for Ce^{3+}- and Li^+-codoped $MSiN_2$. It is interesting to note that the Ce^{3+} ion shows absorption in the UV-blue range (around 400 nm) in both $SrSiN_2$ and $BaSiN_2$ hosts. However, compared to the high absorption of Eu^{2+} in the wavelength range of 300–530 nm in $MSiN_2$, Ce^{3+} only shows a weak absorption in the wavelength range of 370–420 nm. The increase in Ce^{3+} concentration hardly enhances this UV-blue absorption, which is attributed to the limited solubility of Ce^{3+} in the host of $MSiN_2$ because more and more secondary phases can be detected by XRD measurements and the lattice parameters of $MSiN_2$ do not change anymore when the doping concentration of Ce^{3+} is above 2 mol %.

3.3. Photoluminescence Properties of Eu^{2+} in $MSiN_2$ (M = Sr, Ba). Figure 5, parts a and b show the typical emission spectra of $Sr_{1-x}Eu_xSiN_2$ and $Ba_{1-x}Eu_xSiN_2$ ($0 < x \le 0.1$), respectively. Eu is present as the divalent ion in both Eu-doped $BaSiN_2$ and $SrSiN_2$ samples due to the absence of sharp f−f transition lines characteristic for Eu^{3+} in their emission spectra. As a result, all the broad emissions in the sample of $M_{1-x}Eu_xSiN_2$ ($0 < x \le 0.1$; M = Sr, Ba) are essentially assigned to the $4f^65d^1 \rightarrow 4f^7$ transition of the Eu^{2+} ion on the single M site. $Sr_{1-x}Eu_xSiN_2$ ($0 < x \le 0.1$) shows a broad emission band in the wavelength range of 550–850 nm with maxima from 670 to 685 nm with an increase in the Eu^{2+} concentration, while the sample of $Ba_{1-x}Eu_xSiN_2$ ($0 < x \le 0.1$) shows a broad emission band in the wavelength range of 500–750 nm with maxima from about 600 to 630 nm with an increase in the Eu^{2+} concentration. The reasons for the red shift will be discussed in detail below.

Typical excitation spectra of $MSiN_2$:Eu^{2+} (M = Sr, Ba) are presented in Figure 6. As for the compound $MSiN_2$ (M = Sr, Ba), there is only one crystallographic M site with 8-fold nitrogen coordination. The point symmetry of M is C_1 for Sr and C_s for Ba. When the Eu^{2+} ion occupies a lattice site with C_1 or C_s symmetry, a splitting into five 5d bands is expected in the excitation spectra of Eu^{2+}-doped $MSiN_2$ (M = Sr, Ba) samples. Due to serious overlap, only three dominating 5d bands can be observed in the excitation spectra of Eu^{2+}-doped $MSiN_2$ (M = Sr, Ba) besides a shoulder excitation band with a peak center at about 300 nm. These three dominated 5d bands are located at about 340, 395, and 465 nm, respectively. The position of these excitation bands is not largely dependent on the type of the M ions and the

(37) Yamashita, N. N. *J. Phys. Soc. Jpn.* **1973**, *35*, 1089.

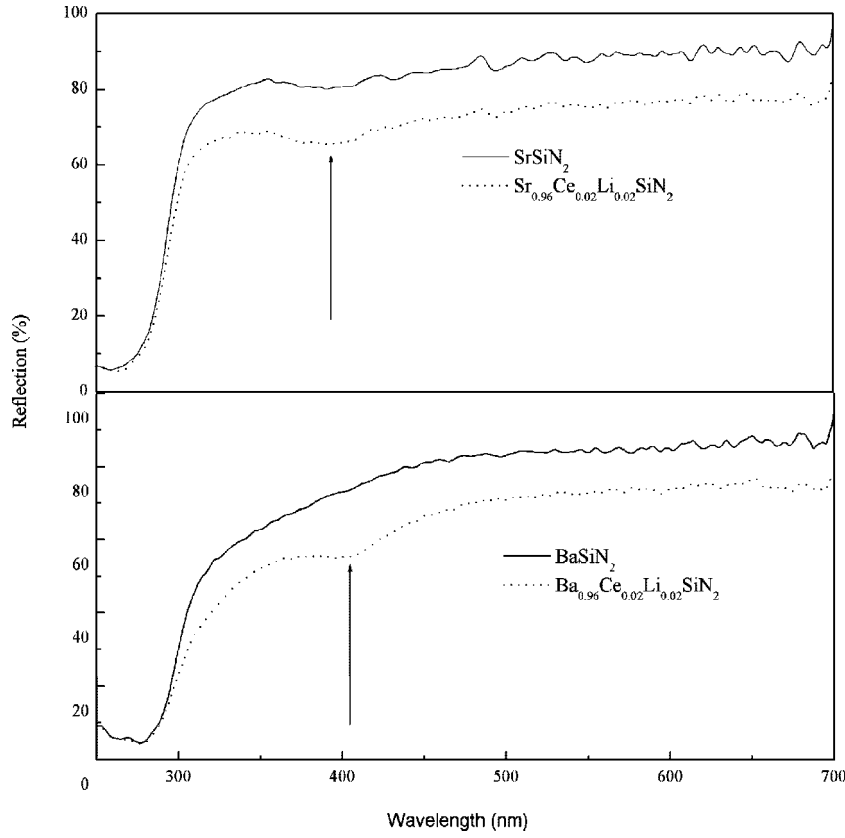

Figure 4. Diffuse reflection spectra of $M_{0.96}Ce_{0.02}Li_{0.02}SiN_2$ (M = Sr, Ba).

Eu^{2+} concentration. Only a small variation for Sr versus Ba can be observed, in agreement with the observed diffuse reflection spectra. Several weak excitation bands below 275 nm are readily assigned to the host lattice excitation (e.g., transition from the valence to conduction band for the $MSiN_2$ host lattices). The weak appearance of the excitation bands of the host lattice in the excitation spectrum of Eu^{2+} indicates that there exists some energy transfer from host lattice to Eu^{2+} ions. The host lattice defects may play an important role on this energy transfer process. It is believed that a small amount of oxygen originating from the raw materials or the oxidation of raw materials during the process of transfer from the glovebox to the furnace will be incorporated on the N site in Eu^{2+}-doped $MSiN_2$ (M = Sr, Ba). Thus, the defect of $(O_N)^{\bullet}$ will be formed. Considering the charge compensation of O substitution on N sites, some other cation vacancies such as $(V_M)''$ have to be formed. Upon UV excitation of the host lattice, these defects may serve as carrier traps by capturing electrons or holes. It is reasonable to assume that $(O_N)^{\bullet}$ will capture electrons, while $(V_M)''$ will capture holes. Hence, when $MSiN_2:Eu^{2+}$ is excited by UV light absorbed by the host lattice, there are possibly two mechanisms for the transfer of energy from the host lattice to the activators (Eu^{2+}). One is the direct transfer from the host to Eu^{2+}. In this case, the energy transfer is due to electron–hole pair recombination followed by transfer of the resulting energy to a nearby Eu^{2+} ion or due to the recombination of electrons with holes trapped by Eu^{2+}. The other mechanism is the energy transfer from the host to Eu^{2+} via the donor–acceptor pairs. Following excitation, the generated electrons and holes are trapped by a donor [like $(O_N)^{\bullet}$] and an acceptor [like $(V_M)''$], respectively. Upon recombination, the energy is transferred from the donor–acceptor pair to Eu^{2+}. The remaining excitation bands in the wavelength range of 300–550 nm clearly originate from the $4f^7 \rightarrow 4f^65d^1$ transition of Eu^{2+}. The most intense 5d excitation band of Eu^{2+} is located at about 395 nm in $MSiN_2:Eu^{2+}$. The lowest energy levels of the 5d excitation band (very broad at about 420–550 nm) seem to show some fine structure, especially for M = Sr at higher Eu^{2+} concentrations. The 5d excitation band of the Eu^{2+} ions at lower energy (>400 nm) is attributed to the influence of highly covalent bonding of $M_{Eu}-N$ and a large crystal-field splitting due to the presence of nitrogen.[4,38] The crystal-field splitting estimated from the energy difference between the highest and lowest observed 5d excitation levels of Eu^{2+} is calculated to be about 11 200 cm^{-1} for $SrSiN_2$ and 10 500 cm^{-1} for $BaSiN_2$, assuming no 5d sub-bands to be positioned in the conduction band of the host lattice.

Here, it is worth noting that $MSiN_2:Eu^{2+}$ (M = Sr, Ba) has not only high absorption but also efficient excitation in the same spectral region of 300–530 nm, perfectly matching with the radiative light from the InGaN- or GaN-based LEDs. Thus, the luminescence properties of $MSiN_2:Eu^{2+}$ (M = Sr, Ba) are favorable for white LED applications.

The red shift in the emission spectrum is frequently observed in rare-earth-doped phosphors as the dopant level increases.[3,20,21,24] Several phenomena can contribute to such a red shift, such as the change of crystal field strength, Stokes

(38) van Krevel, J. W. H.; Hintzen, H. T.; Metselaar, R.; Meijerink, A. *J. Alloys Compd.* **1998**, *268*, 272.

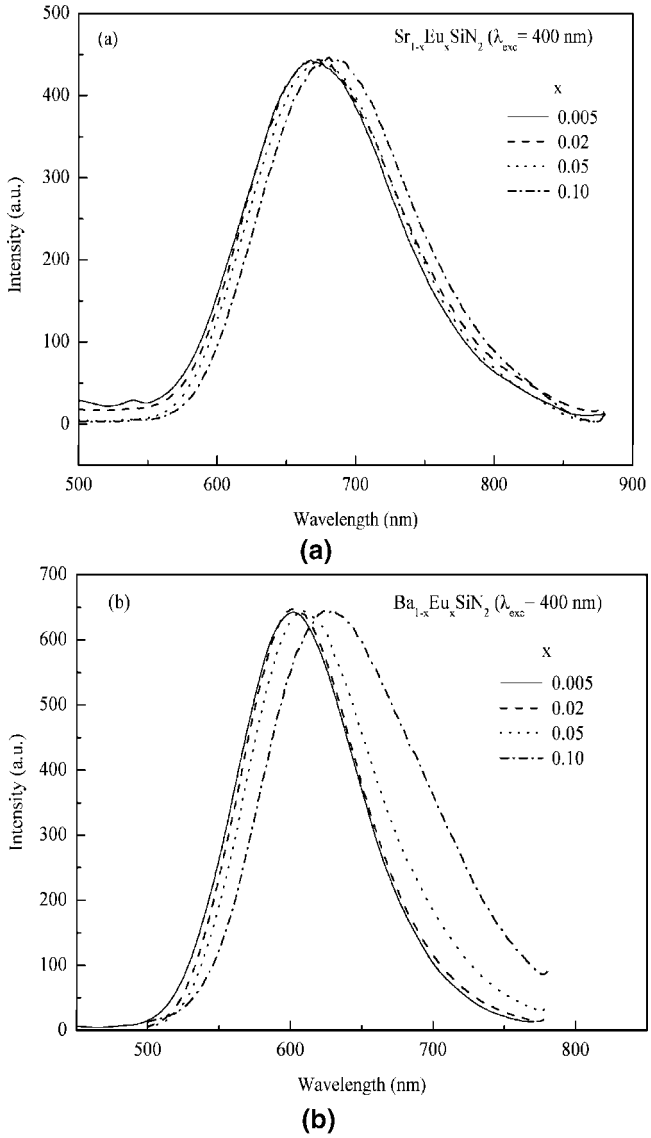

Figure 5. Emission spectra of $M_{1-x}Eu_xSiN_2$ under an excitation wavelength of 400 nm: (a) M = Sr, (b) M = Ba.

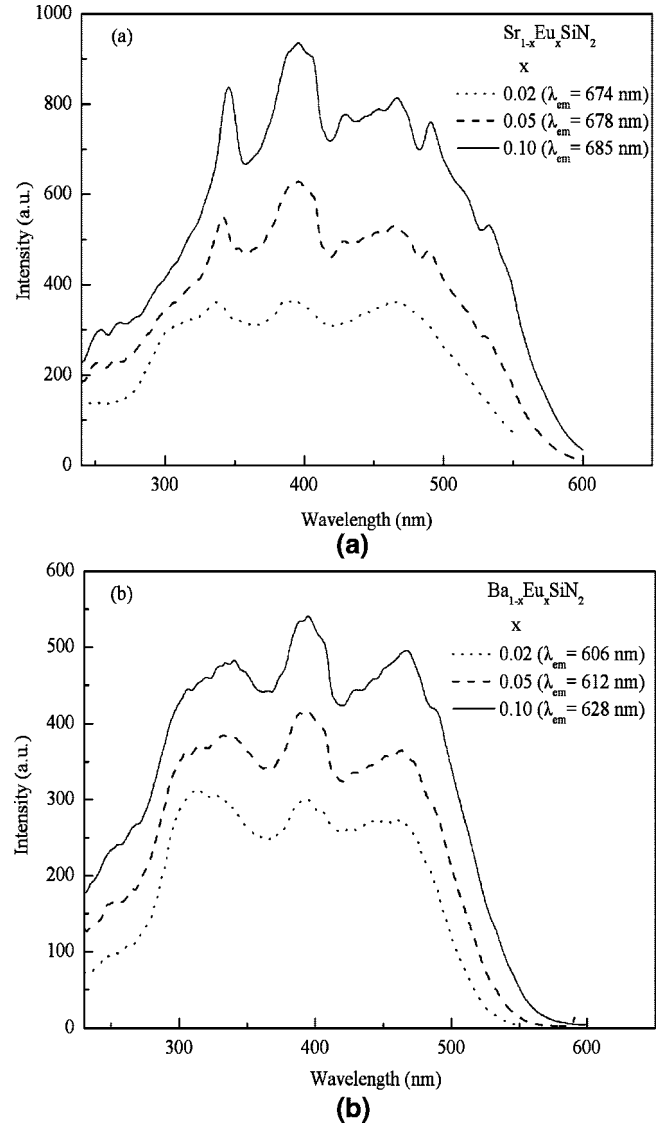

Figure 6. Excitation spectra of $M_{1-x}Eu_xSiN_2$: (a) M = Sr, (b) M = Ba.

shift, reabsorption, and so on. It is often ascribed to the changes in crystal field strength surrounding the activators[3,20,21,24] because the incorporation of dopants into the lattice would cause the expansion or shrinkage of the unit cell, and consequently changes in bond length, covalency, and possibly also symmetry. One of the phenomenological characteristics of the variation of the crystal field strength is the significant change in the position and shape of the excitation band. However, in our case, the excitation spectrum hardly varies except for intensity changes as a function of the Eu^{2+} concentration, indicative of no significant changes in crystal field strength. Figure 7 shows the Stokes shift calculated from the energy difference between the lowest 5d excitation level and emission band of Eu^{2+} as a function of the Eu^{2+} concentration in the host of $SrSiN_2$ and $BaSiN_2$, respectively. It is clearly seen that the Stokes shift increases with an increase in the Eu^{2+}concentration. Based on the fact that the crystal field strength does not change greatly, the observed red shift is therefore dominantly attributed to the increased Stokes shift. Of course, some additional contribution of reabsorption to the observed red shift cannot be ruled out.[3,20,21,24]

Figure 7 also shows the emission intensity of $M_{2-x}Eu_xSiN_2$ ($0 < x \leq 0.1$; M = Sr, Ba) as a function of Eu^{2+} concentration under an excitation wavelength of 400 nm. For both $SrSiN_2$ and $BaSiN_2$, the optimal emission intensity is observed for the material doped with 2 atom % Eu^{2+} (i.e., $x = 0.02$). The emission intensity declines intensively as the concentration of Eu^{2+} exceeds 2 atom % due to concentration quenching.

Figure 8 shows the comparison between the luminescence properties of the $MSiN_2:Eu^{2+}$ (2%) phosphors and those of the commercial LED phosphor $YAG:Ce^{3+}$ under the same measurement conditions. From the comparison, we can see that $MSiN_2:Eu^{2+}$ can be efficiently excited in an even broader excitation wavelength range (300–530 nm) as compared to $YAG:Ce^{3+}$. Under an excitation of 450 nm, the absolute emission intensity is about 35% for $BaSiN_2:Eu^{2+}$ and 15% for $SrSiN_2:Eu^{2+}$ relative to that of $YAG:Ce^{3+}$. By correcting for the differences in absorption, the quantum efficiency is calculated to be about 40% for $BaSiN_2:Eu^{2+}$ and 25% for $SrSiN_2:Eu^{2+}$ relative to that of $YAG:Ce^{3+}$. The quantum

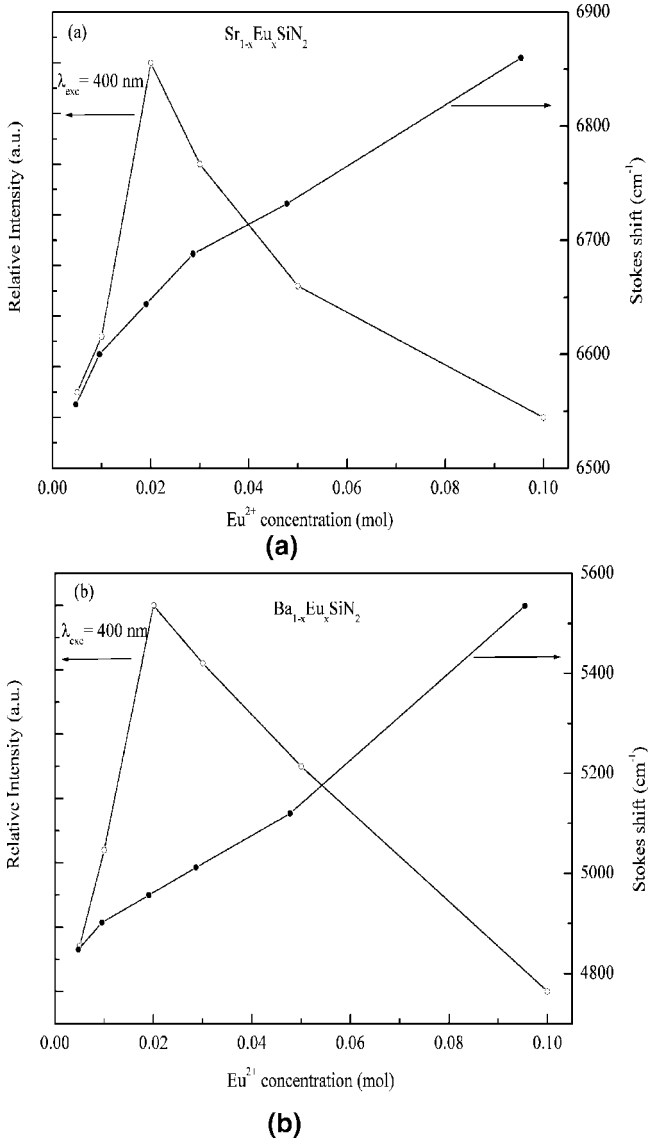

Figure 7. The emission intensities of $M_{1-x}Eu_xSiN_2$ under an excitation wavelength of 400 nm and the changes in Stokes shift as a function of the Eu^{2+} concentration: (a) M = Sr, (b) M = Ba.

efficiency is already high for nonoptimized phosphors but still has to be increased further to increase their potential for white LED lighting applications.

Table 1 summarizes the composition, phase characteristics, and luminescence properties of Eu^{2+}-doped $MSiN_2$ (M = Mg, Ca, Sr, Ba) for a comparison. The luminescence properties of Eu^{2+}-doped $MSiN_2$ (M = Mg, Ca, Sr, Ba) are influenced by the crystal structure of the host lattice and the size of the M ion. For the compounds of $SrSiN_2$ and $BaSiN_2$ with similar structure, there is only a single crystallographic M site with 8-fold nitrogen coordination. The metal–ligand (Eu−N) distance is smaller in $SrSiN_2$:Eu^{2+} than in $BaSiN_2$:Eu^{2+} because Ba^{2+} is larger than Sr^{2+}.[39] As a consequence, the crystal field strength and 5d splitting should be larger for Eu^{2+} in $SrSiN_2$ than in $BaSiN_2$, which is indeed experimentally found, as shown in Table 1. Moreover, according to the configurational coordinate diagram for Eu^{2+}, the relaxation of the Eu^{2+} ion in the excited-state is expected

(39) Shannon, R. D. *Acta Crystallogr., Sect. A* **1976**, *32*, 751.

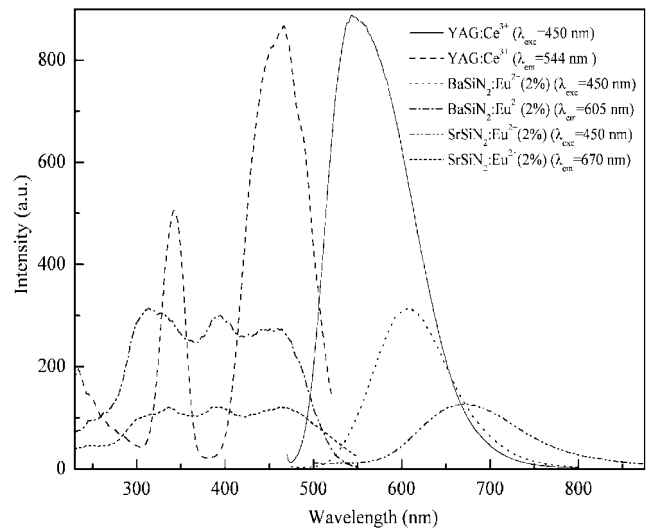

Figure 8. The luminescence properties of $MSiN_2$:Eu^{2+} (2%) (M = Sr, Ba) phosphors compared with those of the commercial LED phosphor YAG:Ce^{3+} under the same measurement conditions.

to be larger for Eu^{2+} in $SrSiN_2$ than in $BaSiN_2$, because Eu^{2+} shrinks during excitation, which is more obstructed on the larger Ba^{2+} site than on the Sr^{2+} site.[40–42] Normally, this results in a larger Stokes shift for Eu^{2+} on a Sr^{2+} site versus a Ba^{2+} site in isostructural compounds,[40–42] which is also observed for Eu^{2+} in $MSiN_2$ (M = Sr, Ba; Table 1). Both effects (i.e., crystal field strength and Stokes shift) may be able to explain why the emission of Eu^{2+} in $SrSiN_2$ is at a lower energy (i.e., longer wavelength) than in the $BaSiN_2$ host lattice. For $MgSiN_2$:Eu^{2+} and $CaSiN_2$:Eu^{2+} in this respect, even higher emission wavelengths are expected for Eu^{2+}, which however is not the case (Table 1). Probably, these deviations are related to the fact that the crystal structures of $MgSiN_2$ and $CaSiN_2$ are different from that of $MSiN_2$ (M = Sr, Ba), and the fact that strong local distortion will occur for the large Eu^{2+} ion incorporated on a small Ca^{2+} and, in particular, Mg^{2+} site.

3.4. Photoluminescence Properties of Ce^{3+} in $MSiN_2$ (M = Sr, Ba). Figure 9 shows typical excitation and emission spectra of $SrSiN_2$:Ce^{3+}/Li^{+}. The sample displays a broad emission band in the wavelength range of 400–700 nm with a peak center at about 534 nm. Generally speaking, the emission band of Ce^{3+} ions shows doublet character due to the spin–orbit splitting of the ground state ($^2F_{5/2}$ and $^2F_{7/2}$) with an energy difference of about 2200 cm^{-1}.[43] In Figure 9, it can be seen that the emission curves of $SrSiN_2$:Ce^{3+}/Li^{+} are not really split. Nevertheless, as shown in the inset of Figure 9, this broad emission band can be decomposed into two well-separated Gaussian components with maxima at about 19 800 and 17 500 cm^{-1} (corresponding to 505 and 570 nm, respectively) with an energy difference of about 2300 cm^{-1}. Moreover, the full-widths at half-maximum (FWHM) of the two Gaussian components are both about 2300 cm^{-1}. It is believed that Ce^{3+} will replace Sr^{2+} on the

(40) Blasse, G. J. *Chem. Phys.* **1969**, *51*, 3529.
(41) Blasse, G.; Bril, A. *Philips Tech. Rev.* **1970**, *31*, 314.
(42) Meijerink, A.; Blasse, G. *J. Lumin.* **1989**, *43*, 287.
(43) Blasse, G.; Grabmaier, B. C. *Luminescent Materials*; Spring-Verlag: Berlin, 1994.

Table 1. Composition, Phase Characteristics, and Photoluminescence Properties of Eu^{2+}-Doped $MSiN_2$ (M = Mg, Ca, Sr, Ba) at Room Temperature

$M_{1-x}Eu_xSiN_2$	M = Mg ($0 < x \leq 0.15$)	Ca	Sr ($0 < x \leq 0.1$)	Ba ($0 < x \leq 0.1$)
phase	$MgSiN_2$	$CaSiN_2$	$SrSiN_2$	$BaSiN_2$
body color			light orange to orange	yellow to orange
crystal system	*Pna*2$_1$	*F*4*b*3*m*	*P*2$_1$/*c*	*Cmca*
number of M sites	1		1	1
host lattice band gap (eV)	4.8	4.5	4.2	4.1
absorption bands of Eu^{2+} (nm)	275–410		300–530	300–530
Eu^{2+} 5*d* excitation bands (nm)	277 ± 2, 293 ± 2, 316 ± 2, 340 ± 2, 375 ± 2		306 ± 2, 336 ± 2, 395 ± 2, 466 ± 2	312 ± 2, 334 ± 2, 395 ± 2, 464 ± 2
emission band maximum (nm)	517	620	670–685	600–630
crystal field splitting (cm^{-1})[a]	≈9400		≈11200	≈10500
stokes shift (cm^{-1})[b]	≈7300		≈6500–6900	≈4850–5550
relative quantum efficiency (%)[c]			25%	40%
ref	14, 15	12	this work	this work

[a] Crystal-field splitting estimated from the energy difference between the highest and lowest observed 5d excitation levels of Eu^{2+}. [b] Stokes shift calculated from the energy difference between the lowest 5d excitation level and emission band of Eu^{2+}. [c] The relative quantum efficiency of the nonoptimized $MSiN_2$:Eu^{2+} (2 mol %) phosphors under an excitation of 450 nm determined as compared to the commercial LED phosphor YAG:Ce^{3+}.

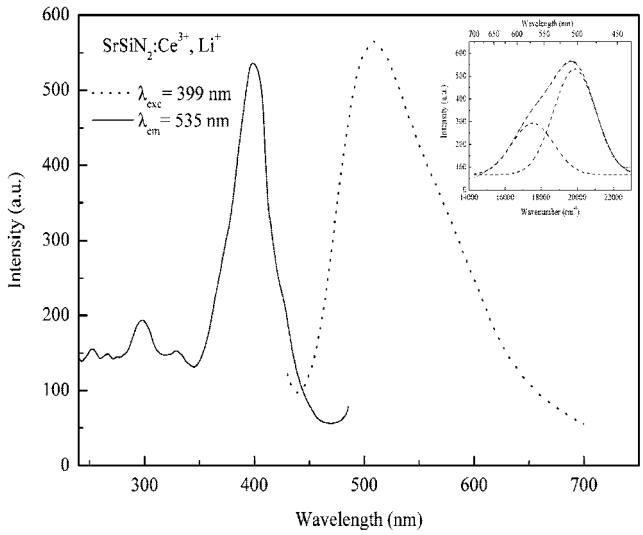

Figure 9. Typical excitation and emission spectra of $SrSiN_2$:Ce^{3+}/Li^+. The dashed curves (inset) represent the two decomposed Gaussian components for the emission spectrum of $SrSiN_2$:Ce^{3+}/Li^+ on an energy scale.

single crystallographic site available in $SrSiN_2$ (Table 2) with some kind of charge compensation. The success of fitting two Gaussian components with an energy difference of 2300 cm^{-1} attributed to the transition from the lowest 5d level to the $^2F_{5/2}$ and $^2F_{7/2}$ levels indicates that mainly one luminescent Ce^{3+} center is present in $SrSiN_2$:Ce^{3+}/Li^+. Three distinct bands can be observed with maxima at 298, 330, and 399 nm, respectively, plus several weak excitation bands below 275 nm in the excitation spectrum of $SrSiN_2$ (Figure 9). Definitely, these weak excitation bands below 275 nm originate from the host lattice, which has also been observed in the excitation spectra of Eu^{2+}-doped $MSiN_2$ samples (Figure 6). The remaining excitation bands in the wavelength range of 275–450 nm are assigned to Ce^{3+} 4f → 5d transitions separated by crystal field splitting of the 5d state. The crystal field splitting of the 5d state and Stokes shift of Ce^{3+} ion in the host of $SrSiN_2$ were calculated to be about 8500 and 6350 cm^{-1}, respectively.

Figure 10 shows typical excitation and emission spectra of $BaSiN_2$:Ce^{3+}/Li^+. The sample exhibits a broad emission band in the wavelength range of 400–700 nm with a peak center at about 486 nm. Similar to the broad emission band of Ce^{3+} in the host of $SrSiN_2$, this broad emission can also be well decomposed into two well-separated Gaussian components with maxima at about 20 700 and 17 000 cm^{-1} (corresponding to 483 and 582 nm, respectively) on an energy scale (inset in Figure 10). The energy difference between 20 700 and 17 000 cm^{-1} is 3700 cm^{-1}, which does not match with the normal ground-state splitting of Ce^{3+} (≈ 2200 cm^{-1}). Moreover, their FWHM are about 2900 cm^{-1} for the 17 000 cm^{-1} peak and 3400 cm^{-1} for the 20 700 cm^{-1}, which are obviously different. Therefore, this suggests that more than one luminescent Ce^{3+} center is present in $BaSiN_2$:Ce^{3+}/Li^+ with different local environments, for example, due to a difference in charge compensation (i.e., with or without lithium in their vicinity) or due to different local cooridinations for Ce^{3+} in $BaSiN_2$:Ce^{3+}/Li^+ as a consequence of local distortion because Ce^{3+} is much smaller than Ba^{2+}. Two distinct excitation bands are detected with maxima around 305 and 403 nm, respectively, plus several weak excitation bands below the wavelength range of 275 nm. Similar to the case of $SrSiN_2$:Ce^{3+}/Li^+, these weak excitation bands and the remaining excitation bands in the wavelength range of 275–450 nm are assigned to the host lattice excitation and Ce^{3+} 4f → 5d transitions separated by crystal field splitting of the 5d state, respectively. The crystal field splitting of the 5d state and Stokes shift of Ce^{3+} in the host of $BaSiN_2$ were calculated to be about 8000 and 4300 cm^{-1}, respectively. Table 2 summarizes the composition, phase characteristics, and luminescence properties of Ce^{3+}- and Li^+-codoped $MSiN_2$ (M = Ca, Sr, Ba) for a comparison. Similar to the reasons for the larger Stokes shift and longer wavelength emission of Eu^{2+} in $SrSiN_2$ than in the $BaSiN_2$ host lattice (section 3.3), Ce^{3+} also shows a larger Stokes shift and longer wavelength emission in $SrSiN_2$ than in the $BaSiN_2$ host lattice.

Finally, it is worthwhile to mention that the absorption and the excitation bands of $MSiN_2$:Ce^{3+}/Li^+ perfectly match with the radiation of the InGaN-based LEDs in the range of 370–420 nm; so in combination with other phosphors, these materials are capable of generating white light. However, an increase in absorption in the range of 370–420 nm will improve their potential for white LED applications.

Table 2. Composition, Phase Characteristics, and Typical Photoluminescence Properties of Ce^{3+}- and Li^{+}-Codoped $MSiN_2$ (M = Ca, Sr, Ba) at Room Temperature

	M		
$MSiN_2:Ce^{3+}/Li^{+}$	Ca	Sr	Ba
phase	$CaSiN_2$	$SrSiN_2$	$BaSiN_2$
crystal system	face-centered cubic	*P*21/*c*	*Cmca*
number of M sites		1	1
body color	pink/red	gray-white	gray-white
host lattice band gap (eV)		4.2	4.1
absorption bands of Ce^{3+} (nm)	450–550	370–420	370–420
Ce^{3+} 5d excitation bands (nm)	365, 390, 440, 535	298, 330, 399	305, 403
emission band maximum (nm)	625	535	485
crystal fields splitting (cm^{-1})[a]	≈8700	≈8500	≈8000
stokes shift (cm^{-1})[b]	≈2700	≈6350	≈4300
ref	13	this work	this work

[a] Crystal-field splitting estimated from the energy difference between the highest and lowest observed 5d excitation levels of Ce^{3+}. [b] Stokes shift calculated from the energy difference between the lowest 5d excitation level and emission band of Ce^{3+}.

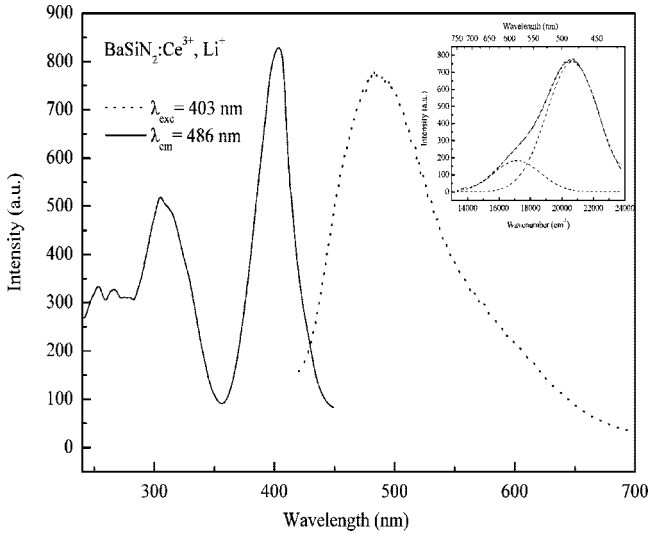

Figure 10. Typical excitation and emission spectra of $BaSiN_2:Ce^{3+}/Li^{+}$. The dashed curves (inset) represent the two decomposed Gaussian components for the emission spectrum of $BaSiN_2:Ce^{3+}/Li^{+}$ on an energy scale.

5. Conclusion

The luminescence properties of Eu^{2+} and Ce^{3+} in $MSiN_2$ (M = Sr, Ba) host lattices were investigated. Eu^{2+}-doped $MSiN_2$ (M = Sr, Ba) shows a broadband emission in the spectral range from orange to deep red (600–690 nm). With increasing Eu^{2+} concentration, the emission band of $MSiN_2:Eu^{2+}$ (M = Sr, Ba) shifts to a long wavelength depending on the type of M ion and the Eu^{2+} concentration. This red shift is attributed to an increase of the Stokes shift and reabsorption by Eu^{2+}. The high absorption and strong excitation bands of $MSiN_2:Eu^{2+}$ (M = Sr, Ba) in the wavelength of 300–530 are very favorable properties for white LED applications. The quantum efficiency of $MSiN_2:Eu^{2+}$ is already high for nonoptimized phosphors but has to be increased further for making them potential LED conversion phosphors. Ce^{3+}- and Li^{+}-codoped $MSiN_2$ (M = Sr, Ba) exhibits a broad emission band in the wavelength range of 400–700 nm with a peak center at about 485 nm for $BaSiN_2$ and about 535 nm for $SrSiN_2$. Although the absorption and the excitation bands of $MSiN_2:Ce^{3+}/Li^{+}$ perfectly match with the radiation of the InGaN-based LEDs in the range of 370–420 nm, their absorption has to be increased to increase their potential for white LED lighting applications.

Acknowledgment. The authors wish to thank M. M. R. M. Hendrix for his support with XRD measurements, H. A. M. van der Palen for maintenance of the furnaces, and Leuchtstoffwerk Breitungen GmbH Company (Germany) for financial support.

CM701875E